

Nondestructive Testing of GFRP Composite Bridge Decks Using Active Infrared Thermography

Udaya B. Halabe, Ph.D., P.E.

Teaching Professor
School of Sustainable Engineering and the Built Environment (SSEBE)
Arizona State University
Tempe, AZ, USA
udaya.halabe@asu.edu

Ruben M. Joshi, P.E.

Project Engineer
Dewberry
132 West 31st Street, Suite 301
New York, NY, USA
rubenjoshi097@gmail.com

Abstract— Aging of reinforced concrete bridge decks is one of the major problems faced by the engineering community today, with concrete cracking and the steel reinforcement corroding due to exposure to deicing chemicals, thus resulting in shorter service life. An alternative to the degrading bridge decks made of concrete and steel is the use of Glass Fiber Reinforced Polymer (GFRP) composite bridge decks, which are noncorrosive. Use of GFRP bridge decks can lead to enhanced durability. However, ensuring continued structural integrity of GFRP bridge decks requires a reliable method of evaluation for periodic testing in the field environment. Nondestructive Testing (NDT) using Active Infrared Thermography (IRT) can help to detect subsurface defects in GFRP bridge decks that may occur because of vehicular loading and the harsh environmental conditions. Infrared Thermography (IRT) is an extensively used NDT technique for inspection of civil infrastructure, because of its portability and easy-to-handle features. This paper discusses the use of advanced and conventional IRT techniques for detecting subsurface defects in GFRP composite bridge decks. Advanced IRT uses a high-end infrared camera and robust digital image processing software to locate sub-surface defects in GFRP structural members, which, in some cases, conventional IRT technique fails to detect.

Keywords— Infrared Thermography; IRT; Glass Fiber Reinforced Polymer; GFRP; Composites; Debonds; Delaminations

I. INTRODUCTION

Reinforced concrete (RC) bridge decks have been predominantly used in many bridge construction projects. However, the strength of the RC bridge deck is significantly reduced over time due to corrosion in the steel reinforcing bars within the concrete caused by the use of deicing chemicals. Eventually, the deck must be replaced, which is expensive and time-consuming. The use of Glass Fiber Reinforced Polymer (GFRP) composite bridge decks instead of

RC decks for new construction or replacement of old decks is highly desirable. The GFRP composite bridge decks have high stiffness and strength-to-weight ratio and high fatigue and corrosion resistance. In addition to being highly durable, additional benefits of light weight, rapid field construction and easier transportation are offered by the GFRP composite bridge decks [1]. Despite the higher initial cost of GFRP composite bridge decks, their minimal maintenance cost helps in achieving substantial cost savings over the bridge deck's service life [1].

During the manufacturing of GFRP composite bridge decks and their subsequent use in the field (under action of vehicular loads and the harsh environment), some subsurface defects, such as cracks, debonds, delaminations, and voids, could be formed. Such subsurface defects could also be formed during the construction process. These subsurface defects can adversely affect the strength of the GFRP composite bridge deck. Thus, it is important to evaluate the condition of GFRP composite bridge decks and locate and rectify any subsurface defects in a timely manner. Nondestructive Testing (NDT) techniques have been found to be very effective in the inspection of FRP composites. Infrared thermography (IRT) is one of the most frequently used NDT methods that has proven to be successful in detecting subsurface anomalies in GFRP composites [2-6]. The conventional method of infrared imaging, in general, includes heating the test surface and evaluating the still (single snapshot) thermal images that provide information on any subsurface discontinuity through contrast in surface temperature distribution. Flash Thermography (also called Pulsed Thermography) is one of the most widely used infrared thermography techniques in inspection of structural components. This technique is based on fast uniform heating, variable capture rates and wide range of software analysis options [3]. Flash Thermography gives the assessment of the subsurface condition faster than other nondestructive methods. With advancement in analysis techniques, flash or pulsed thermography provides improved ability to determine deeper and more subtle subsurface anomalies [3]. Advanced methods of infrared thermography, such as

Thermographic Signal Reconstruction (TSR), have come into frequent use in structural evaluation in recent years. TSR is a thermography technique where raw temporal data recorded for each pixel in the thermal image is reconstructed with reduction in noise and optimization of thermal contrast [6-9]. This paper compares the effectiveness of conventional and advanced infrared thermography (based on TSR) in detection of debonds and delaminations in GFRP composite bridge decks.

An expensive advanced infrared imaging equipment with integrated flash-lamps based heating system and data processing unit was used for laboratory evaluation of several GFRP bridge deck specimens using the TSR technique. In addition, a low-cost conventional infrared camera was used. The results obtained from the two infrared thermography systems allowed comparison between the efficiencies of the advanced and conventional infrared thermography systems. The laboratory setup, experimentation and analysis results are discussed in the following sections.

II. INFRARED THERMOGRAPHY EQUIPMENT

The advanced infrared imaging equipment (VoyageIR Pro) consisted of a system of hardware and software components (Figure 1). The hardware included the inspection head with infrared camera, computer-controlled heating source, and a tablet computer with touchscreen monitor, all of which were mounted on a tripod stand (Figure 1a) and connected by cables to an Input/Output (I/O) Controller box (Figure 1b). The miniature long-wave uncooled microbolometer infrared camera included a 14.25mm lens with a 640x480 pixels Focal Plane Array (FPA) and image capture frequency of 30Hz (30 frames per second). It detected radiation in the spectral range of 8 to 14 microns. The heat source consisted of an array of fully synchronized miniature heat lamps with precise control over key parameters like pulse width and amplitude. The heat flux from the heat source was 800 W/m^2 at a distance of 24" (0.61m). The integrated 10" (0.25m) touchscreen tablet computer's display featured a streamlined software user interface that provided complete control and remote system operation. However, the backbone of this system was the Input/Output (I/O) System Controller (Figure 1b), which allowed a network of electronics to perform all the major functions, such as heat source synchronization and control, digital data capture and analysis, and trigger I/O. The associated software housed in the tablet computer was an integral part of the system, which was designed to provide a user-friendly interface and easy access to all the program functions. The software allowed capturing and processing of the data with options to set up all the necessary parameters like trigger mode, capture rate and heating time. The thermographic signal reconstruction could be done using the software program which allowed TSR processing and reconstruction of the captured data. The reconstructed

data could be used to obtain raw, 1st and 2nd time-derivative images.

The conventional infrared equipment used for this study was a low-cost handheld infrared camera (Figure 2), which could capture thermal images of a surface with temperatures in the range of -10°C to $+350^\circ\text{C}$ with an accuracy of $\pm 0.1^\circ\text{C}$ at a temperature of 30°C . The 3.5" (0.09m) LCD display on the infrared camera provided a color thermal image with a resolution of 120×120 pixels. This device, weighing 1.21 pounds (0.55 kg), stored thermal images in the format of standard radiometric JPEG files on a removable SD card. These JPEG files could directly be studied to identify debonds. The thermal image files could further be analyzed using the associated software that provided information on minimum, maximum, and average temperatures of a selected area in the image.

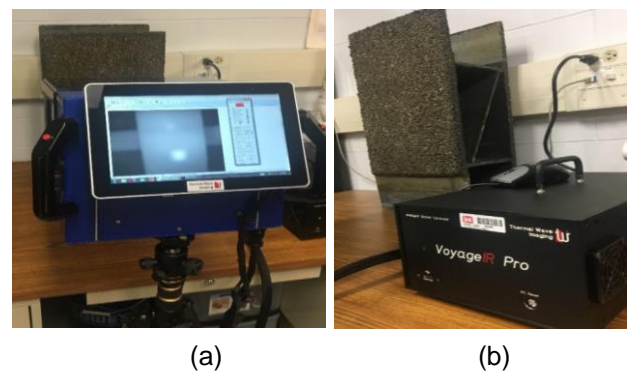


Fig. 1. (a) Inspection Head, and (b) I/O System Controller for Advanced Infrared Imaging Equipment (VoyageIR Pro)



Fig. 2. Low-cost Infrared Camera

III. LABORATORY EXPERIMENTATION

Several GFRP bridge deck specimens, along with embedded defects (debonds and delaminations), were prepared in the laboratory as part of previous research studies [2,4] and were available for this study as well. The bridge deck specimens were prepared by cutting smaller sizes from full size GFRP bridge decks. The depth of the specimens was the same as the full size GFRP deck. Simulated debonds were created by placing artificial defects between the 3/8" (9.5mm) thick polymer concrete wearing surface and the underlying GFRP bridge deck specimen. The delaminations inside the top flange of the decks were

simulated by placing the defects in the middle of the flange joint area. Wax paper was used to cover the defects to keep them intact and a structural adhesive was used to join the two flanges of the adjacent bridge deck modules, resulting in a defect (termed as delamination) inside the flange of the GFRP bridge deck specimen [4,5].

The specimen BD1 was made of E-glass fibers and polyester resin (Figure 3). Its overall plan size was 24" x 12" (0.61m x 0.305m) with an overall depth of 8" (0.2m). The thickness of the flanges was 0.5" (12.7 mm) while that of the web was 0.35" (8.9mm) and of the diagonal members was 0.25" (6.35mm). This composite deck weighed about 15 lb/ft² (73 kg/m²). Air-filled debonds were placed in between the wearing surface and the underlying FRP deck surface. The wearing surface was 3/8" (9.5mm) thick and made of specially selected blend of aggregates, i.e., Glacial Gravel – Basalt, Quartzite and Granite, mixed with two-part liquid polymer system. There were two air-filled debonds of sizes 2" x 2" (51mm x 51mm) and 3" x 3" (76mm x 76mm) on Side 1 of the specimen and two air-filled debonds of sizes 1" x 1" (25mm x 25 mm) and 1/2" x 1/2" (12.7mm x 12.7mm) on Side 2. All the debonds on specimen BD1 were 1/16" (1.6mm) thick.

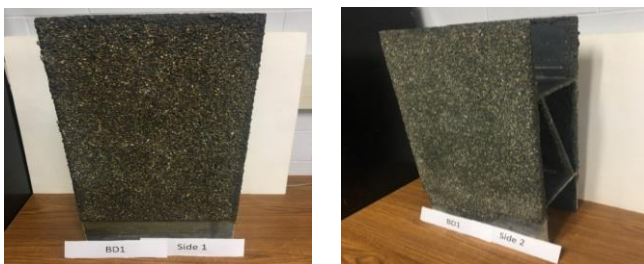


Fig. 3. Side 1 (left) and Side 2 (right) of the GFRP Bridge Deck Specimen BD1

The specimen WJD2 was a low-profile GFRP bridge deck specimen made of E-glass fiber and vinylester resin (Figure 4). The plan size of WJD2 was 24" x 8" (0.61m x 0.20m) with an overall depth of 4" (0.1m). The thickness of the flange was 0.45" (11.4mm) with a thickness of 0.6" (15.2mm) at the flange-to-flange junction. This composite deck weighed about 10 lb/ft² (49 kg/m²). A 3/8" (9.5mm) thick wearing surface, consisting of a two-component polysulphide-epoxy-based overlay system, was applied on Side 2 of the specimen. Both sides of the specimen WJD2 had a water-filled delamination of size 3" x 3" (76mm x 76mm) placed centrally in the flange junction. They were located at 0.32" (8.1mm) from the top of the GFRP deck surface on both sides but Side 2 had an additional 3/8" (9.5mm) thick wearing surface. Side 1 did not have any wearing surface.

The specimen AS3 was also a low-profile 4" (0.1m) thick GFRP bridge deck made of E-glass fiber and vinyl-ester resin, with a plan size of 24" x 12" (0.61m x 0.305m) as shown in Figure 5. Side 1 of specimen AS3 had 3/8" (9.5mm) thick wearing surface which consisted of two-component polysulphide-epoxy-based

overlay system. On Side 1, a 3" x 3" (76mm x76mm) sized air-filled debond of thickness 1/16" (1.6mm) was placed in between the wearing surface and the underlying deck. Side 2 did not have any wearing surface. There was a 3" x 3" (76mm x76mm) thick air-filled delamination with 1/16" (1.6mm) thickness on Side 2 in the flange-to-flange junction.

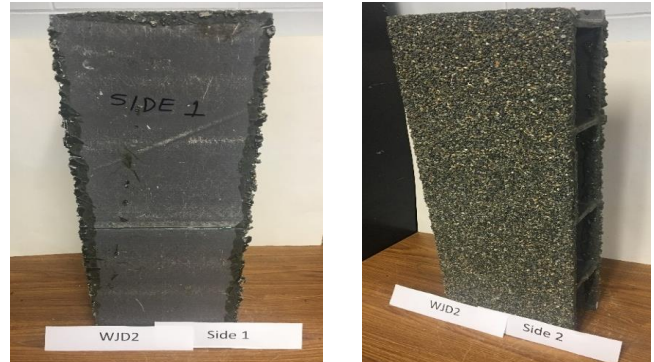


Fig. 4. Side 1 (left) and Side 2 (right) of the GFRP Bridge Deck Specimen WJD2

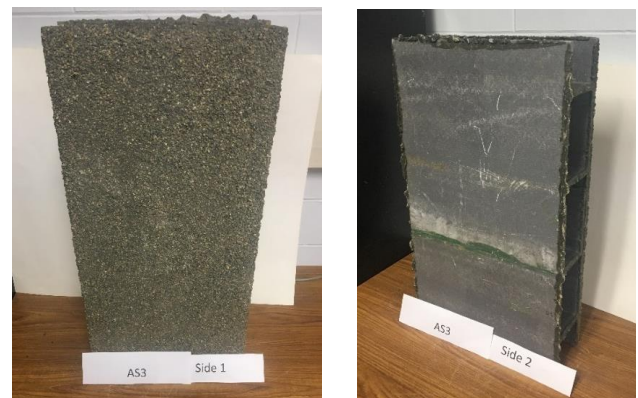


Fig. 5. Side 1 (left) and Side 2 (right) of the GFRP Bridge Deck Specimen AS3

The specimens were placed on the table and the advanced infrared imaging equipment (VoyageIR Pro) was set up on a tripod stand such that the surface of the specimen was at a distance of 24" (0.61m) from the in-built infrared camera of the system, as shown in Figure 1a. The infrared camera on the device was maintained at a height of 42" (1.07m) from the ground to achieve a proper testing setup. The system also had a 9" (0.23m) long shield in the front to prevent any thermal noise from the surrounding while the thermal data from the specimen was being captured. The surface of the specimen was heated for different time durations (50s, 100s, 200s) in different experiments to determine the optimal heating duration (for the GFRP bridge deck specimens) for the VoyageIR Pro, which is an advanced infrared imaging equipment (Figure 1). This system was used to capture the sequence of thermal images (30 frames per second) during the heating process and for 30 seconds after the heating stopped. After the device captured the thermal data and the surface was still in thermally excited state, the low-cost conventional infrared camera (Figure 2) was used to capture still (single shot) thermal image of the surface of the bridge deck specimen.

After capturing the thermal data, the associated software in the advanced infrared imaging system was used to process the captured data to obtain TSR, 1st derivative image and 2nd derivative image. The software provided TSR, 1st derivative and 2nd derivative intensity images at different times in the recording sequence, and the images with the best thermal contrast was used to identify the subsurface defects. The conventional infrared thermography images taken from the low-cost infrared camera gave still images (single time snapshots) of the heated surface. These still images were studied directly to locate the defects. In addition, the associated software for the conventional camera was used to obtain minimum, maximum, and average temperatures of selected areas in the still images (single time snapshots). The results from both infrared systems are presented in the next section.

IV. RESULTS

The infrared thermography testing of bridge deck specimens using advanced infrared imaging system (Figure 1) gave results in the form of TSR images, and 1st and 2nd derivative images. In addition, still images using the conventional infrared camera (Figure 2) were also captured. For 50 seconds of heating, the defects in Side 1 of bridge deck specimen BD1 (air-filled debonds between the wearing surface and the underlying GFRP deck) could be seen in all the images: TSR image, 1st derivative image, 2nd derivative image, and the conventional still image (Figure 6). The defects in the 1st derivative image were sharper than in the other images. For the smaller air-filled debonds in Side 2 of specimen BD1 (Figure 7), only the 1st derivative image showed the defects prominently. The conventional thermal image did not show the defects clearly after 50 seconds of heating. Figures 8 and 9 show the results obtained with 100 seconds of heating for bridge deck specimen BD1. The conventional thermal image indicated that the surface temperature corresponding to the largest defect was 4.5°C higher than the surrounding temperature (Figure 8). Figures 8 and 9 also indicate that the 1st derivative image is the clearest and the most reliable processed image.

For bridge deck specimen WJD2 (with water-filled delamination within the deck flanges), Side 1, with no wearing surface, showed delamination after 50s, 100s, and 200s of heating (Figure 10). However, Side 2 (covered with wearing surface) did not clearly indicate the water-filled defect after 50s of heating (left figure in Figure 11). Only after 100s and 200s of heating, the delamination could be detected, but the boundary of the delamination could not be noted clearly (Figure 11). Figure 12 shows the conventional thermal images of uncovered Side 1 (without wearing surface) of specimen WJD2 after 50s, 100s, and 200s of heating. The 3" x 3" (76mm x 76mm) sized delamination could only be detected after 100s of heating, with the temperature above the delamination being 3.4°C higher than the surrounding areas. The covered Side 2

(with wearing surface) did not show clear indication of the subsurface delamination in conventional thermal images for 50s and 100s heating durations (Figure 13). The infrared image corresponding to 200s heating duration (last image in Figure 13) shows the presence of delamination, but the boundary of the delamination cannot be deciphered. In summary, the 1st derivative images from advanced infrared imaging system could detect subsurface defects better than conventional images from the low-cost infrared camera. Also, the deeper subsurface defects (with wearing surface) required longer duration of heating as compared to the shallow defects (without wearing surface).

Infrared thermography testing of bridge deck specimen AS3 gave results as shown in Figures 14 and 15. The raw images for both sides of AS3 after 50s of heating was not indicative of the defects. The debond on Side 1 and the delamination on Side 2 were clearly visible in the 1st derivative images after 50s of heating. The conventional thermal images of Side 1 and Side 2 also showed the presence of defects (with temperature difference of around 2°C), but the defect boundary was not prominent for Side 2. The processed images (1st derivative image) obtained through TSR technique was very helpful to locate the subsurface defects while the raw images did not show the presence of the defects (Figures 14 and 15).

V. CONCLUSIONS

The nondestructive evaluation of GFRP bridge deck specimens in the laboratory using active infrared thermography enabled the detection of simulated subsurface defects (debonds and delaminations) and led to an assessment of the effectiveness of advanced and conventional infrared thermography testing for different types of GFRP bridge deck specimens. The advanced infrared thermography technique using TSR is a relatively new technique requiring an expensive system compared to the low-cost infrared camera.

The advanced infrared thermography system was very useful since the heating source was embedded in the same unit and the associated data processing capability was very good. In most cases, the raw and TSR images could not detect the subsurface defects, while the processed images (especially the 1st derivative image) were able to identify the defects very clearly. This is because the flanges of the GFRP deck specimens were thick and covered by wearing surface in many cases, and the 1st derivative images were found to be very useful in detecting the subsurface defects. The advanced infrared thermography using 1st derivative images was able to detect the subsurface defects even in situations where conventional thermography was unsatisfactory. In essence, the advanced infrared thermography system proved to be very useful, owing to its excellent heating system and superior data processing capabilities over the conventional infrared camera. Also, use of conventional infrared thermography requires an external heat source which is its major drawback.

The results from laboratory experiments also helped in determining the effectiveness of heating source embedded in the advanced infrared equipment for GFRP bridge deck applications. A heating duration of 100 seconds was found to be appropriate for the current GFRP bridge deck application. The advanced infrared imaging system permitted recording of thermal data throughout the heating process and the recording continued for some time after the heating was stopped (i.e., during cooling cycle). The associated software could simultaneously be used to process the data and obtain reconstructed thermal data. The advanced infrared imaging system with its embedded heating system, along with its powerful data processing capability, was easy to handle and operate.

ACKNOWLEDGMENTS

The authors gratefully acknowledge the support provided by the US Army Corps of Engineers (USACE) by loaning their VoyageIR Pro equipment which enabled the authors to undertake this study when they were at West Virginia University.

REFERENCES

[1] Mara, V., Haghani, R., and Harryson, P. "Bridge Decks of Fiber Reinforced Polymer (FRP): A Sustainable Solution." *Construction and Building Materials*, 50, 2014, pp. 190-199.

[2] Roy, M. "Nondestructive Testing of FRP Structural Components Using Digital Infrared Thermography." MS Problem Report (Advisor: Dr. Udaya B. Halabe), Department of Civil and Environmental Engineering, West Virginia University, Morgantown, WV, USA, August 2004.

[3] Spring, R., Huff, R., and Schwoegler, M. "Infrared Thermography: A Versatile Nondestructive Testing Technique." *Materials Evaluation*, 69(8), August 2011, pp. 934-942.

[4] Vasudevan, A. "Application of Digital Infrared Thermography for Nondestructive Evaluation of Composite Bridge Components." MS Thesis (Advisor: Dr. Udaya B. Halabe), Department of Civil and Environmental Engineering, West Virginia University, Morgantown, WV, USA, May 2004.

[5] Halabe, U. B., Vasudevan, A., Klinkhachorn, P., and GangaRao, H. V. S., "Detection of Subsurface Defects in Fiber Reinforced Polymer Composite Bridge Decks Using Digital Infrared Thermography," *Nondestructive Testing and Evaluation*, 22(2-3), June-Sept., 2007, pp. 155-175.

[6] Shepard, S. M. "Thermographic Characterization of Composites." SAMPE 2013.

[7] Shepard, S. M., and Beemer M .F. "Characterization of Materials using Thermographic Signal Reconstruction." *InfraMation 2015 Proceedings*.

[8] Shepard, S.M., Lhota, J.R., Rubadeux, B.A., Ahmed, T. and Wang, D. "Enhancement and Reconstruction of Thermographic NDT Data." *Thermosense XXIV, Proceedings of SPIE*, Vol. 4710, 2002, pp. 531-535.

[9] Oswald-Tranta, B., Maier, A., and Schledjewski, R. "Defect Depth Determination in a CFRP Structure using TSR Technique." *Proceedings of QIRT 2014, Bordeaux, France, July 7–11*.

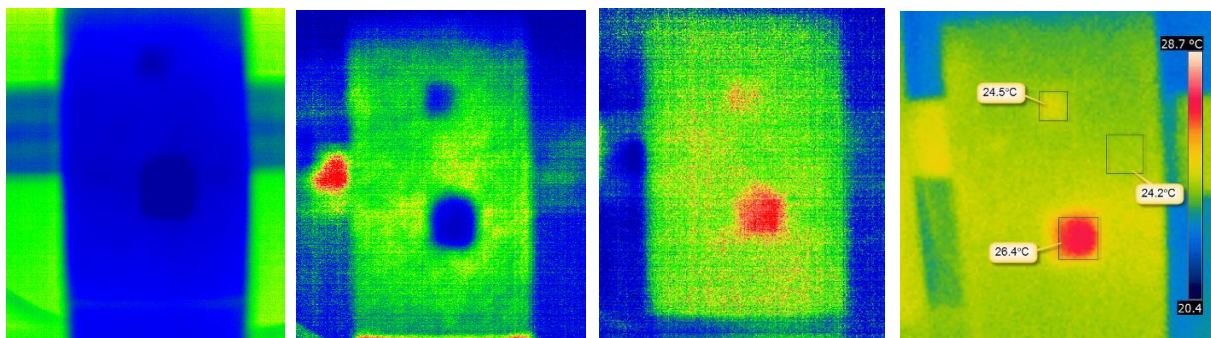


Fig. 6. From left: TSR image, 1st derivative image, 2nd derivative image, and conventional infrared image of Side 1 of the GFRP bridge deck specimen BD1 after 50 seconds of heating

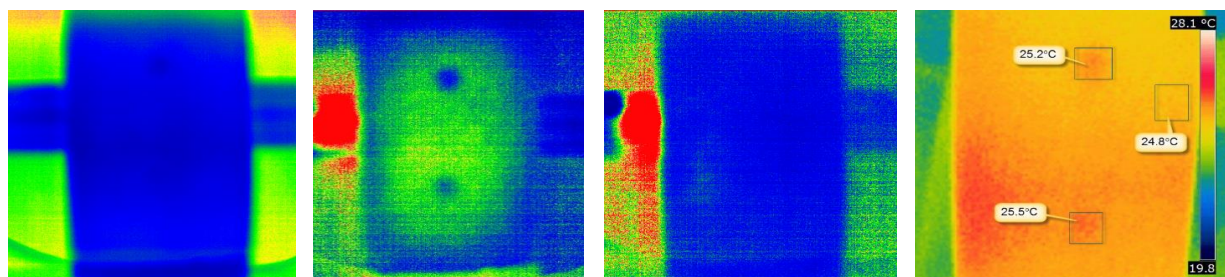


Fig. 7. From left: TSR image, 1st derivative image, 2nd derivative image, and conventional infrared image of Side 2 of the GFRP bridge deck specimen BD1 after 50 seconds of heating

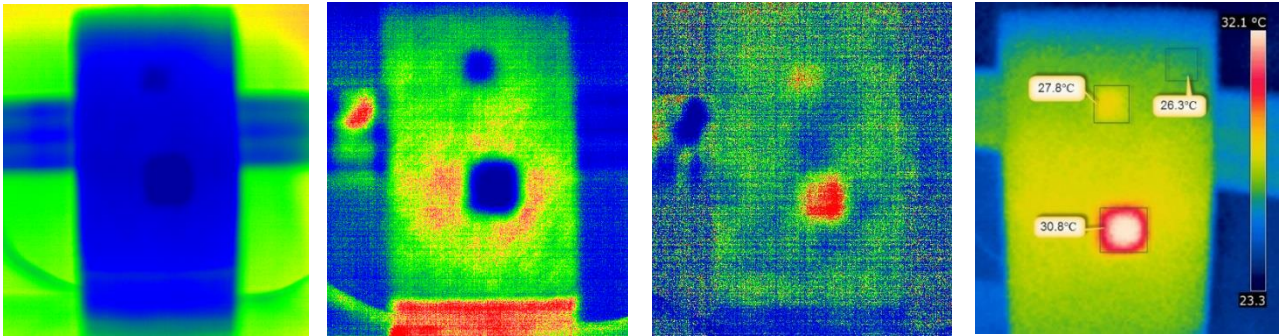


Fig. 8. From left: TSR image, 1st derivative image, 2nd derivative image, and conventional infrared image of Side 1 of the GFRP bridge deck specimen BD1 after 100 seconds of heating

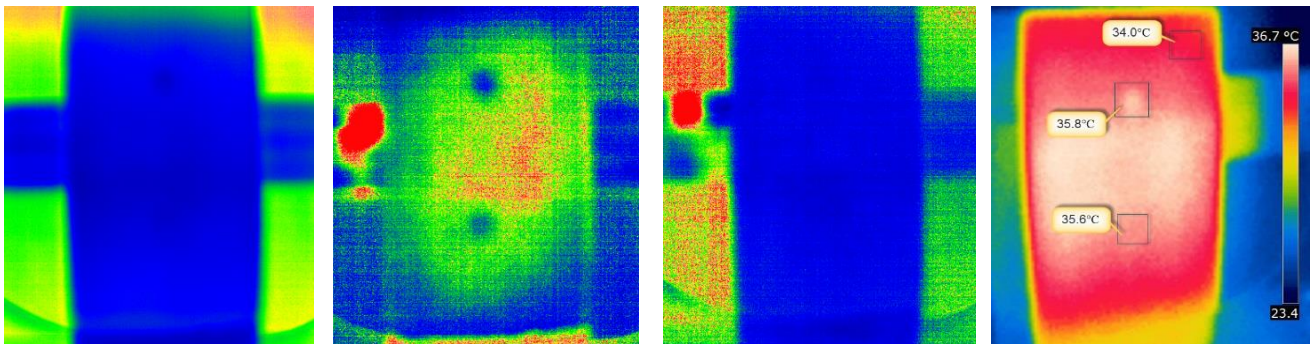


Fig. 9. From left: TSR image, 1st derivative image, 2nd derivative image, and conventional infrared image of Side 2 of the GFRP bridge deck specimen BD1 after 100 seconds of heating

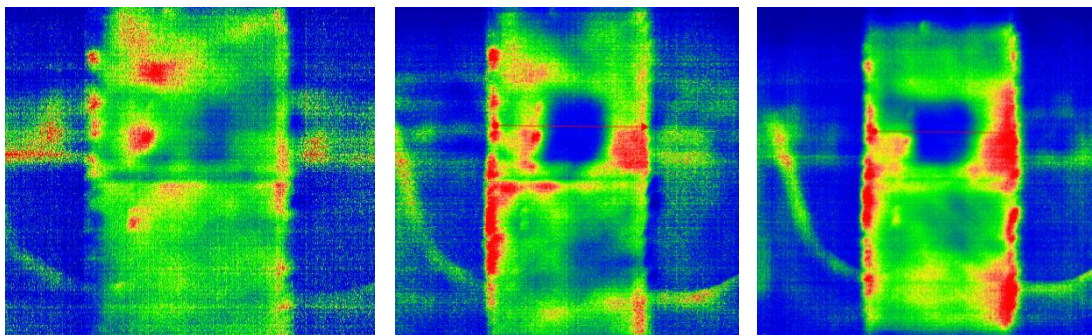


Fig. 10. 1st derivative images of uncovered Side 1 (without wearing surface) of the GFRP bridge deck specimen WJD2 after 50 seconds (left), 100 seconds (center), and 200 seconds (right) of heating

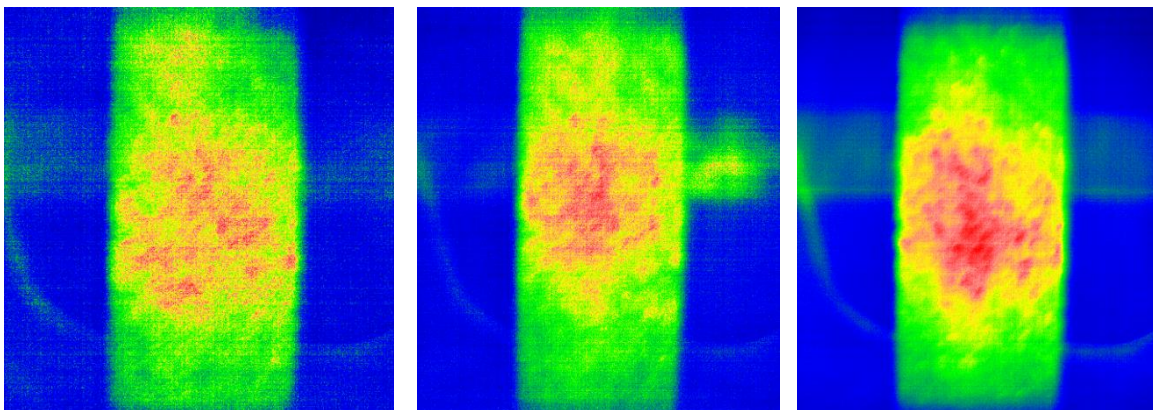


Fig. 11. 1st derivative images of covered Side 2 (with wearing surface) of the GFRP bridge deck specimen WJD2 after 50 seconds (left), 100 seconds (center), and 200 seconds (right) of heating

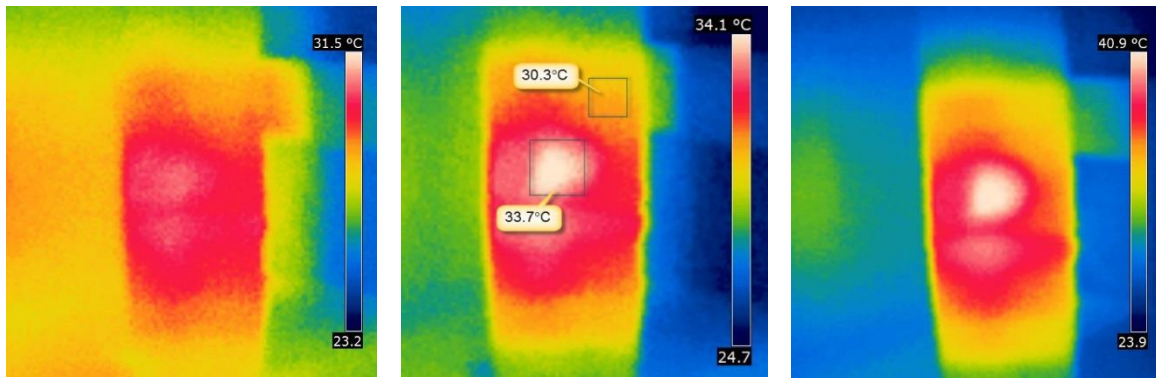


Fig. 12. Conventional thermal images of uncovered Side 1 (without wearing surface) of the GFRP bridge deck specimen WJD2 after 50 seconds (left), 100 seconds (center), and 200 seconds (right) of heating

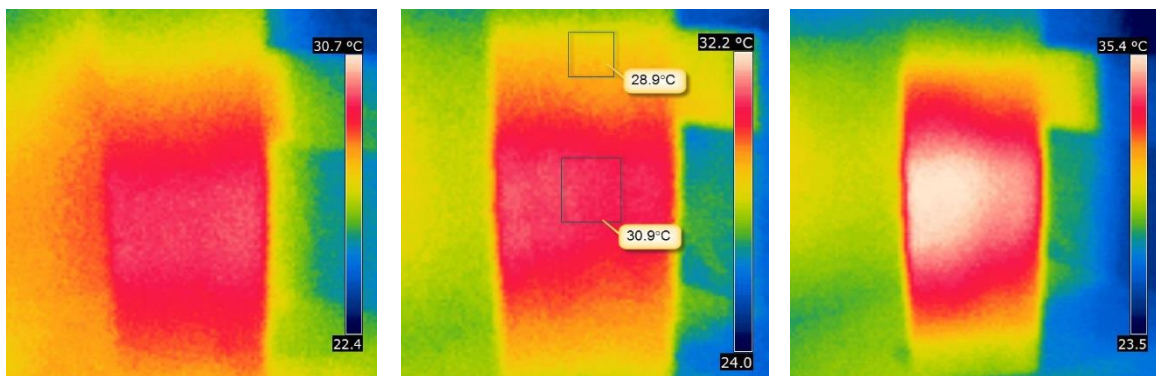


Fig. 13. Conventional thermal images of covered Side 2 (with wearing surface) of the GFRP bridge deck specimen WJD2 after 50 seconds (left), 100 seconds (center), and 200 seconds (right) of heating

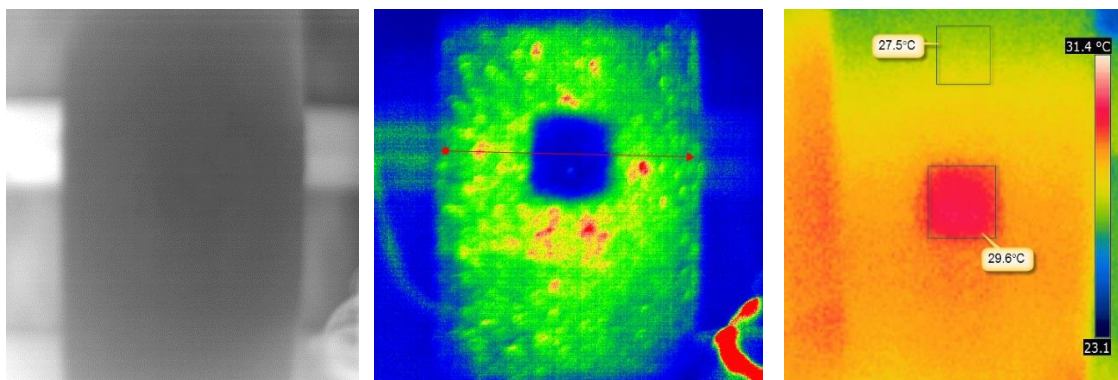


Fig. 14. Raw image (left), 1st derivative image, and conventional thermal images of Side 1 of GFRP bridge deck specimen AS3 after 50 seconds of heating

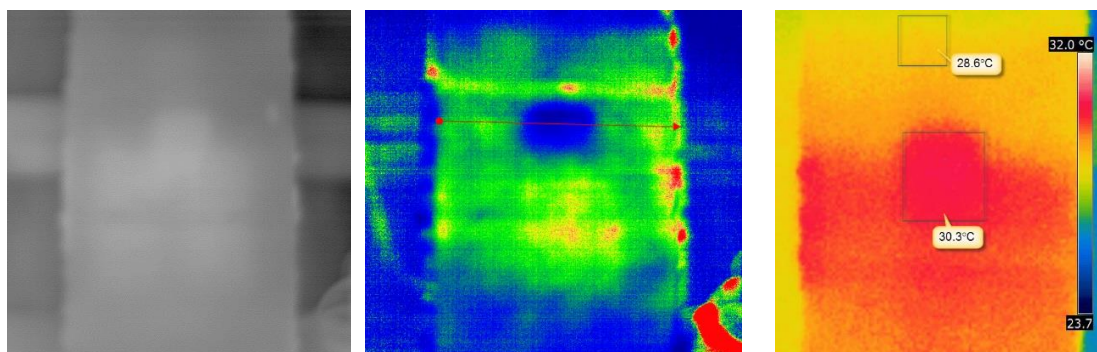


Fig. 15. Raw image (left), 1st derivative image, and conventional thermal images of Side 2 of GFRP bridge deck specimen AS3 after 50 seconds of heating